Physics Letters A 383 (2019) 1084–1091

Contents lists available at ScienceDirect

Physics Letters A

www.elsevier.com/locate/pla

Diffusive transport in highly corrugated channels

Fabio Cecconi [a,*], Valon Blakaj [b], Gabriele Gradoni [b], Angelo Vulpiani [c,d]

[a] CNR-Istituto dei Sistemi Complessi (ISC), Via dei Taurini 19, I-00185, Roma, Italy
[b] School of Mathematical Sciences and George Green Institute for Electromagnetics Research, University of Nottingham, University Park, NG72RD Nottingham, United Kingdom
[c] Department of Physics, Università di Roma "Sapienza", Piazzale A. Moro 5, I-00185 Roma, Italy
[d] Centro Interdisciplinare "B. Segre", Accademia dei Lincei, Via della Lungara, Roma, Italy

ARTICLE INFO

Article history:
Received 9 October 2018
Received in revised form 27 December 2018
Accepted 27 December 2018
Available online 4 January 2019
Communicated by C.R. Doering

Keywords:
Billiards
Ray-optics
Transport
Diffusion
Correlated random-walks

ABSTRACT

Diffusion in waveguides with spatially modulated profiles is an important topic in modern electromagnetics and optics. Wave dynamics in the high-frequency asymptotics are governed by classical ray dynamics which can be characterised by looking at the diffusion of particles throughout the channel. We study the transport of particles (rays) in a channel with a sinusoidal profile at different values of the corrugation amplitude. We find that below a certain corrugation level the transport is ballistic, beyond this threshold, a diffusion-like behaviour emerges in the asymptotic limit of large times. In this regime particle transport slows down due to the trapping mechanism in the corrugated regions of the channel. We use the analogy with correlated random walks to discuss the observed transport regimes.

1. Introduction

Diffusion of waves in corrugated channels is a subject of great interest in optics [1], plasma physics [2] and microwave technology [3]. This problem is relevant in the engineering community to study the effects of spatial modulation of boundaries on wave guides [4]. In optics, understanding and controlling the flow of light is of crucial importance for photonic devices. Photonic crystals and optical fibers exhibit a rich classical dynamics that can be characterised by studying the ray diffusion constant and related phase-space structure [5,6]. The study of particle trajectories is meaningful as they evolve according to geometrical optics (GO) similarly to waves in the high frequency limit.

Classical wave simulations have been proven to be successful for predicting the average energy distribution in both vibro-acoustics [7] and electromagnetic systems [8]. In vibro-acoustics, the so called dynamical energy analysis (DEA) is used to transport classical phase-space distributions along geodesic lines and it provides an estimate of the average vibrational energy of complex built-up structures [8,9]. In this work, we study the deterministic diffusion of particles in channels with sinusoidal profile of arbitrary depth, i.e., beyond the perturbative regime, as a proxy to understand the dynamics of wave diffusion in the high frequency regime, where ray tracing predictions neglects phase information and therefore energy distribution is predicted without accounting for interference.

Billiards with a channel geometry, beside their practical application to the area of optical fibers and waveguides, can be regarded as natural candidates to explain the classical ballistic transport of carriers in quasi-1D dimensional structures [10]. One can also use such models to study the heat conduction in 1-D systems in connection with mass transport [11,12].

Billiard channels also offer the possibility to study the deterministic diffusion in peculiar wall geometries: dispersive walls [13–19] and non-dispersive (i.e. flat) walls such as in polygonal channels [20–22].

Moreover, low-dimensional billiards are Hamiltonian systems simple enough to test fundamental problems of statistical mechanics, for instance, the relationship between microscopic dynamics and transport properties. In this context, a particular emphasis was devoted to track the role of chaos in the deterministic diffusion and to find the origin of possible anomalous behaviours at low dimensionality. In particular, several works on polygonal billiards [20,21] contributed to further clarify the scenario for which even non-chaotic systems (with zero Lyapunov exponent) are able to display robust normal diffusion. [23,24].

* Corresponding author.
E-mail address: fabio.cecconi@roma1.infn.it (F. Cecconi).

https://doi.org/10.1016/j.physleta.2018.12.041

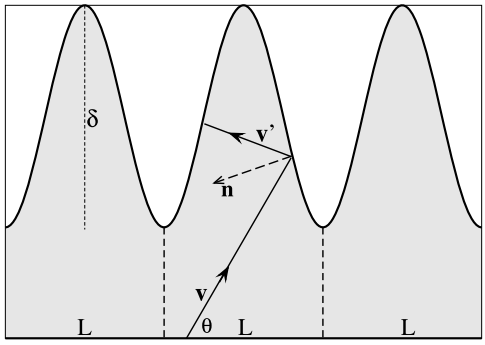

Fig. 1. Pictorial representation of a periodically corrugated channel geometry. Thick vertical dashed lines delimit the fundamental cell around the origin. The lines with the arrows indicate the specular reflection of the trajectories with respect to the normal **n**. In this picture, the cell size (period) is $L = 3$, we set $w_0 = 1$ and the corrugation parameter $\delta = 2$. In the following, only δ will be varied.

In general, billiard channels are neither completely chaotic nor integrable systems, so regions of regular and chaotic motion coexist in their phase-space, it is, thus, interesting to study the diffusion in the presence of KAM tori that constitute impenetrable barriers to the motion [25].

The channel we consider here extends existing works on corrugated channels [17–19] to the extreme regime of high corrugations: a situation where particles/rays may experience relevant trapping effects.

The knowledge gained by the dynamical system analysis of waveguide structures in the ray approximation (wavelength of light λ much smaller than all the geometrical parameters of the system) is useful to select the optimal geometrical properties of waveguide-based resonators, micro lasers and multiply interconnected cavities.

The paper is organized as follows. Sec. 2 describes the corrugated channel and the billiard dynamics of the particles and the possible transport regimes. Simulation results and their interpretation are presented in Sec. 3. Finally Sec. 5 is devoted to conclusions where we give some remarks on the infinite horizon and its implication on our results.

2. Model, geometry and transport regimes

In this section we derive the map of particles/rays traveling through a channel with an arbitrary corrugation amplitude. The system we study is depicted in Fig. 1, and it consists of a corrugated channel where independent point particles travel ballistically until they undergo specular reflections from the boundaries. Collisions off the transverse modulation profile scatter the trajectories and generate longitudinal spreading of particles. The geometry of the channel is defined such that the bottom boundary is flat and placed at $y = 0$, whereas, the top boundary is the periodic profile

$$w(x) = w_0 + \frac{\delta}{2}\left[1 + \cos(kx)\right], \tag{1}$$

where, $k = 2\pi/L$, with L being the channel period (longitudinal size of the unit cell), w_0 is the minimal channel, δ determines the corrugation amplitude. The channel is open, in the sense that particles can escape to the infinity along the x-direction (infinite horizon).

Consider the case where the velocity modulus is $|\mathbf{v}| = 1$, and particles experience reflections from the flat bottom wall at $y = 0$ and the rippled top wall $w(x)$.

Both, the position $\mathbf{x}_n = \mathbf{x}(t_n)$ and the velocity $\mathbf{v}_n = \mathbf{v}(t_n)$ of a particle are updated after each collision with the walls according to the mapping

$$\mathbf{x}_{n+1} = \mathbf{x}_n + \mathbf{v}_n h_n, \tag{2}$$

$$\mathbf{v}_{n+1} = \mathbf{v}_n - 2\,(\mathbf{v}_n \cdot \mathbf{e}_{n+1})\,\mathbf{e}_{n+1} \tag{3}$$

where, h_n is the time between two consecutive impacts of the particle trajectory with the boundaries. Whereas, the $\mathbf{e}_n$ denotes the unitary normal evaluated at the impact point either on flat boundary $\mathbf{e}(x) = (0, 1)$ or on the corrugated profile (1)

$$\mathbf{e}(x) = \left[\frac{w'(x)}{\sqrt{1 + w'(x)^2}}\,,\ \frac{-1}{\sqrt{1 + w'(x)^2}}\right], \tag{4}$$

$w'(x)$ stands for $dw(x)/dx$. The (time) h_n is found by solving the transcendental equation

$$y_n + b_n h_n = w(x_n + a_n h_n)\,, \tag{5}$$

with (x_n, y_n) and (a_n, b_n) denoting the positions and the velocity components emerging from the (last) n-th collision. Eq. (5) has been solved numerically by using a bisection algorithm with an absolute error tolerance 10^{-14}.

It is more practical to reformulate the elastic reflection of velocities after the impact in a linear algebra notation

$$v'_\alpha = v_\alpha - 2\,e_\alpha \sum\nolimits_\beta v_\beta e_\beta,$$

with Greek subscripts denoting x, y components and v' the post-impact velocity. The above expression can be recast as

$$v'_\alpha = \sum\nolimits_\beta M_{\alpha\beta} v_\beta,$$

where the matrix, $M_{\alpha\beta} = \delta_{\alpha\beta} - 2\,e_\alpha e_\beta$, according to Eq. (4) takes the simple expression

$$M = \begin{bmatrix} \dfrac{2}{1+m^2} - 1 & \dfrac{2\,m}{1+m^2} \\ \dfrac{2\,m}{1+m^2} & 1 - \dfrac{2}{1+m^2} \end{bmatrix}, \tag{6}$$

we set $m = w'(x)$. The matrix formulation of collision is particularly easy to be numerically implemented as, for each given x, only two elements need to be assigned, that is $M_{xx} = -M_{yy} = c - 1$ and $M_{xy} = M_{yx} = cm$, with $c = 2/(1 + m^2)$. By setting $m = 0$, one obtains the reflection rule with the flat boundary.

The symplectic character of the mapping (3) reflects onto its transport properties which will be certainly related to the KAM structure of the phase-space especially for small δ: $\delta \ll w_0$, [17, 26,18,19].

The case $\delta = 0$, corresponding to the integrable limit, leads to the trivial map

$$x_{n+1} = x_n + h\,\cot(\theta_n), \qquad \theta_{n+1} = \theta_n\,,$$

implying the conservation of the horizontal velocity in the $n-$th flight $v\cos(\theta_{n+1}) = v\cos(\theta_n)$ and the inversion of transversal velocity. This behaviour is characterized by a purely ballistic transport $\sigma^2(t) \sim t^2$.

An even small corrugation, $\delta \ll w_0$, introduces a perturbation of the integrable system leading to a more complex map

$$x_{n+1} = x_n + \Delta x_n, \qquad \theta_{n+1} = \theta_n + \Delta\theta_n\,, \tag{7}$$

where both Δx_n and $\Delta\theta_n$ depend on the position of the collision on the boundaries, and they are determined numerically via Eqs. (5). In this case, the investigation needs the direct simulation of dynamics (3).

The limit of small δ has been addressed by many authors [17, 26,18] who were able to work out the explicit form of the map (7). These papers, mainly addresses the KAM properties of the phase

space and escape statistics, however, did not consider the explicit exploration of diffusion-like behaviours.

The situation becomes more complex when the corrugation is enough to allow multiple inversion of the v_x component.

The role of the parameter δ in the dynamics can be summarized as follows. Once the profile (1) is recast in the dimensionless form $\omega(\xi) = 1 + d\cos(\xi)$, with $d = 1/(1 + 2w_0/\delta)$ and $\xi = kx$, the ratio w_0/δ not only controls the deviation from the non-integrability of the system but it also weights the importance of the horizon effects. Small w_0/δ implies the "dominance" of the corrugated regions (traps) over the rectangular corridor where transport takes place. In our discussion, w_0 is kept fixed to $w_0 = 1$.

In the next section we will focus on the regime $\delta \gg \delta_c$, which, to our knowledge, is poorly covered by the literature, trying to establish the dependence of the coefficient D_{eff} on δ.

3. Simulation results

We study the transport properties of a large ensemble of M independent particles whose dynamics along the channel has been obtained by iterating the dynamics (3).

The particles are initialized in the state (x_0, y_0, θ_0) such that: x_0 is extracted from a uniform distribution in $[-L/2, L/2]$, $y_0 = 0$ and velocities $|\mathbf{v}| = 1$. The angle, θ_0, that any initial velocity forms with the channel axis is uniformly drawn in the interval $[\theta_a, \theta_b]$, where $\theta_a = \arctan[1/(x_0 - L/2)]$ and $\theta_b = \pi - \arctan[1/(x_0 + L/2)]$. In practice, the particles are launched from the flat boundary of the fundamental cell toward its corrugated wall (see Fig. 1). This choice guarantees that particles undergo the first collision in the initial cell so to avoid, at least at the beginning, extremely long collision-free paths due to the infinite-horizon condition.

The simulations were performed in a spirit closer to the molecular dynamics, where particles are advanced with a time step δt sufficiently small. When a particle exits the channel, it is reinjected according to the mirror symmetry with respect to the tangent line of the profile at the impact point taken as symmetry axis. If a particle after the symmetry operation is still outside the channel the procedure is repeated till the particle lies inside.

We start from the computation of the mean collision time $\langle\tau\rangle$ of two successive elastic collisions with the boundary walls of the channel; in our case of unitary velocity, $\langle\tau\rangle$ coincides with the mean-free path. Such information allows us to understand the scale of times (lengths) involved in the bouncing ball dynamics when parameter δ is varied. It is also a check for the accuracy of the simulation code. According to Refs. [27,28], $\langle\tau\rangle$ can be derived from a simple geometric formula

$$\langle\tau\rangle = \pi\,\frac{A}{P}, \tag{8}$$

with P being the collision perimeter, and A the accessible area of the billiard table. In the case of our channel, the area and the perimeter of a fundamental cell are respectively, $A = L(1 + \delta/2)$ and

$$P = L + 2\int_0^{L/2} dx\sqrt{1 + w'(x)^2}\,,$$

in the above expression, we used the arc-length formula along the corrugated profile.

After a simple manipulation P is expressed as

$$P = L + \frac{2L}{\pi}\int_0^{\pi/2} dz\,\sqrt{1 + \epsilon^2\sin^2(z)}\,,$$

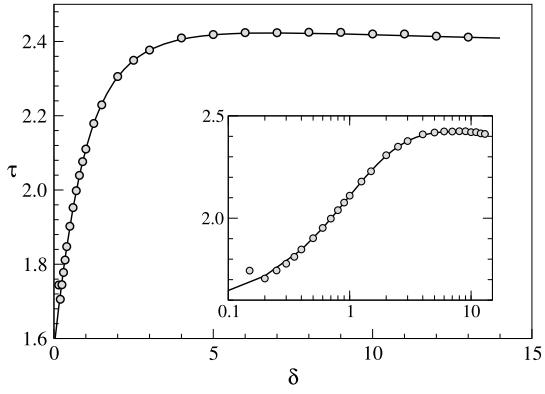

Fig. 2. Behaviour of the mean collision time (mean free-path) with δ. Points indicate simulation data, obtained for a system of $M = 2 \times 10^4$ independent particles; the curve represents the theoretical prediction from Eq. (9) in striking agreement with simulations. Inset: the same plot in log-linear scale.

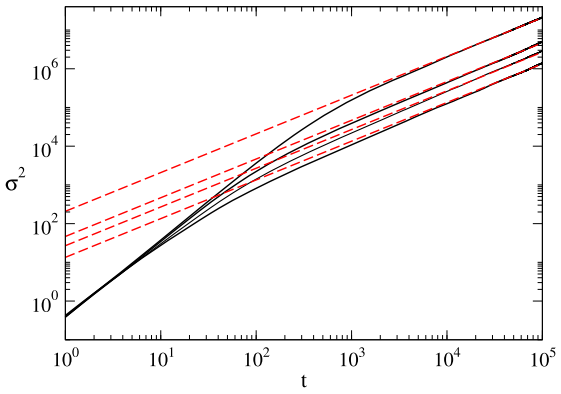

Fig. 3. Log–log plot of the mean square displacement σ^2 behaviour with time at $\delta = 0.2, 0.3, 0.4, 0.5$, from top to bottom. The figure shows the crossover from a transient ballistic motion to a diffusive one. Of course, the crossover time t_*, see Eq. (11), depends on the corrugation parameter δ.

where $\epsilon = \pi\delta/L$ and the integration is a complete elliptic integral of the second kind $E(-\epsilon^2)$ [29]. The final result reads

$$\langle\tau\rangle = \pi\,\frac{2\pi + L\epsilon}{2\pi + 4\,E(-\epsilon^2)}\,. \tag{9}$$

The dependence of the mean collision time $\langle\tau\rangle$ on δ is shown in Fig. 2 which illustrates the agreement between simulation data (points) and the exact expression (9) (line). The match is quite striking also considering that no parameters have to be tuned.

The impact of δ on the transport along the channel axis is evident by the behaviour the mean square displacement,

$$\sigma^2(t) = \langle[x(t) - x(0)]^2\rangle,$$

where, $\langle\cdots\rangle$ denotes an ensemble average over initial conditions. Simulations show that for a channel with $w_0 = 1$ and $L = 3$, there are basically two regimes. For δ smaller than a certain threshold approximately located around $\delta_c \simeq 0.07$, there is a certain dominance of motions characterized by a ballistic asymptotics $\sigma^2(t) \sim t^2$. On the contrary, for $\delta > \delta_c$ chaotic behaviour is prevailing, therefore we observe a diffusion-like behaviour

$$\sigma^2(t) \sim 2D_{\text{eff}}t\,. \tag{10}$$

The value of δ_c can be obtained only numerically. Fig. 3 shows $\sigma^2(t)$ for δ slightly above δ_c. The coexistence of ballistic motion (associated to KAM islands) and irregular (chaotic) motion reflects into the two regimes

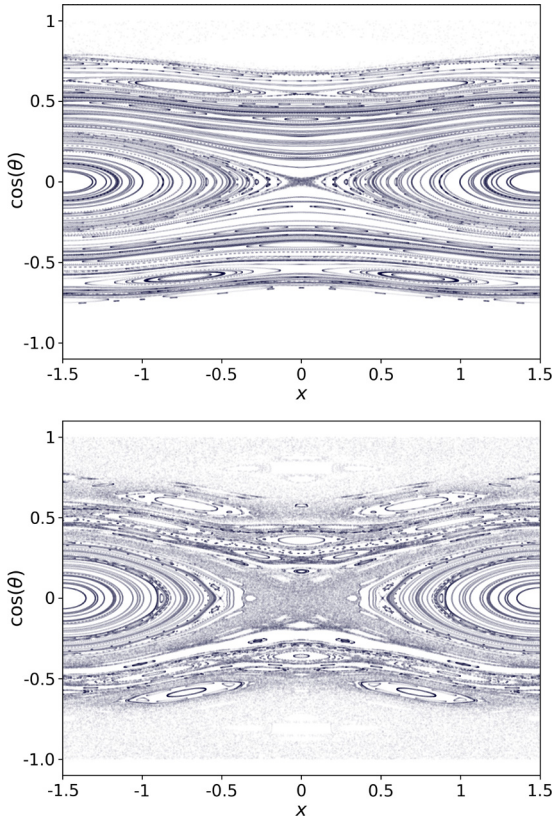

Fig. 4. Poincaré sections on the surface $y = 0$ for $\delta = 0.05$ (top) at which simulations indicate that ballistic behaviour is prevailing; the phase portrait is characterized by the presence of many periodic islands responsible for ballistic motion. While at $\delta = 0.07$ (bottom), the presence of a non negligible chaotic sea allows for irregular motions which can give rise to diffusive-like behaviour. We can consider $\delta = 0.07$ a crossover value for the corrugation separating ballistic and diffusion-like behaviour.

$$\sigma^2(t) \sim \begin{cases} t^2 & \text{for } t < t_*(\delta) \\ t & \text{for } t > t_*(\delta) \end{cases}, \tag{11}$$

where the crossover time t_* is a function of δ which diverges as soon as δ is close to the threshold δ_c.

The presence of the critical value δ_c can be also "visually" verified by plotting, the Poincaré section $[x_n, v_n = \cos(\theta_n)]$ generated by the collisions of the trajectories with the border $y = 0$ (Fig. 4).

If the ripple of the channel is around δ_c, the phase-space portrait is overwhelmed by the periodic islands corresponding to the regular "bouncing ball" orbits in the transverse direction, these determine the ballistic behaviour of $\sigma^2(t)$.

When $\delta > \delta_c$, the emergence of a not negligible chaotic-sea surrounding the periodic islands is responsible for onset of the linear growth of $\sigma^2(t)$.

The diffusive transport of the particle in the channel directions can be quantified by the effective coefficient D_{eff} referring to an initially localized ensemble of particles. D_{eff} is computed by fitting the asymptotic behaviour 10.

Fig. 5 reports the variation of D_{eff} as a function of the corrugation depth δ. D_{eff} turns out to be a monotonic decreasing function of δ showing two qualitatively different trends at small and relatively large corrugation. In the region of small corrugation, $\delta < 0.5$, D_{eff} is very sensitive to the variation of δ and it seems to develop a divergence-like behaviour for small values, which can be roughly estimated from the data as

$$D_{\text{eff}} \sim (\delta - \delta_c)^{-2}, \tag{12}$$

indicated by the first dashed line in Fig. 5. This is consistent with the presence of the threshold δ_c below which the contribution of

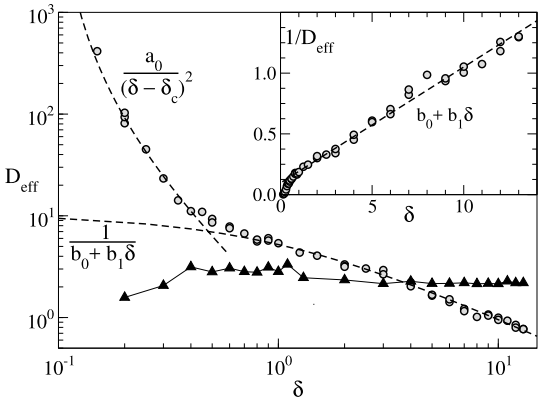

Fig. 5. Behaviour of the effective diffusion coefficient D_{eff} against channel corrugation degree δ in log–log scale. An overall monotonic decrease with increasing δ results in a crossover between two different behaviours. For $\delta > 1$, $D_{\text{eff}} \sim 1/(b_0 + b_1\delta)$, with $b_0 \simeq 0.0964$ and $b_1 \simeq 0.0954$. Whereas for $\delta < 0.5$ the coefficient seems to develop a divergence which can be roughly estimated as $D_{\text{eff}} \sim a_0(\delta - \delta_c)^{-2}$, with $a_0 = 1.05$ and $\delta_c \simeq 0.09$. For a comparison, we plot the prefactor $D_0 = \langle\tau^2\rangle/(2\langle\tau\rangle)$ in Eq. (19) (black triangles), in the jargon, corresponding to the random phase approximation RPA or quasilinear approximation, QLA. The inset shows the same data plotted in the reciprocal y-axis to assess the linear trend $b_0 + b_1\delta$ of the denominator.

a small fraction of ballistic trajectories is sufficient to lead to a superdiffusive behaviour of the MSD.

This scenario somehow recalls the one occurring in the Standard Map (SM) wherein, for values of the control parameter below the threshold, $k < k_c \sim 0.9716\ldots$, the variation of the momentum p is bounded by the presence of KAM tori. The diffusive growth $\langle p^2\rangle \sim D_0 t$ is observed only for $k > k_c$, when even the last KAM torus is destroyed and the chaotic motion can invade the phase space. Analogously in our channel, the presence of KAM tori for $\delta < \delta_c$ corresponds to a ballistic motion, and normal diffusion occurring above δ_c corresponds to the destruction of the last KAM tori. This picture is consistent with the Chirikov's *resonance overlap mechanism* that provides a simple criterium to explain the arising of chaotic zones in the phase space [30]. In the case of SM, the Chirikov's criterion enables to provide a theoretical estimate of the threshold value, however in our case, the criterion is of difficult applicability, so we had to obtain δ_c only by numerical simulations, which suggest a value $\delta_c \approx 0.07$.

The main panel of Fig. 5 and the inset show that in the regime of higher corrugation ($\delta > 1$) the diffusion coefficient decreases with a law

$$D_{\text{eff}} = \frac{1}{b_0 + b_1\delta}. \tag{13}$$

This behaviour can be explained via an heuristic argument which will be presented in the next section. Of course for lower range of δ, D_{eff} can also depend on the finer details of the profile $w(x)$, therefore in these cases, the expression of D_{eff} is not expected to be as simple as Eq. (13).

4. Interpretation of results

In order to understand the behaviour of the coefficient D_{eff}, it is reasonable to look at the motion in terms of *persistence*, which is a natural effect in the context of deterministic diffusion [31,32].

In fact, the correlation that necessarily exists among consecutive free-paths cannot be neglected and confers a certain degree of persistence to the trajectories. Therefore, looking at particle trajectories as correlated random walks [33,34] is particularly useful as we can adapt a derivation developed in Ref. [35] to obtain the well-known Taylor–Green–Kubo formula for D_{eff}.

After n-collisions with the walls, a single particle which started at $\mathbf{x}_0$, is found at the position

$$\mathbf{x}_n = \mathbf{x}_0 + \sum_{i=1}^{n} \mathbf{v}_i \tau_i \,,$$

hence, the average MSD from the initial condition is

$$\langle |\mathbf{x}_n - \mathbf{x}_0|^2 \rangle \simeq \sum_{i,j=1}^{n} \langle \tau_i \tau_j \rangle \, \langle \mathbf{v}_i \cdot \mathbf{v}_j \rangle . \tag{14}$$

This is only valid under the hypothesis of independence between velocity and time. Furthermore, the above sum can be easily rearranged as it follows

$$\langle |\mathbf{x}_n - \mathbf{x}_0|^2 \rangle \simeq \sum_{i=1}^{n} \langle \tau_i^2 \rangle \, \langle \mathbf{v}_i^2 \rangle + 2 \sum_{i,j>i}^{n} \langle \tau_i \tau_j \rangle \, \langle \mathbf{v}_i \cdot \mathbf{v}_j \rangle \,.$$

Now by taking into account that velocities have constant and unitary modulus ($v_0^2 = 1$), $\langle \mathbf{v}_i \cdot \mathbf{v}_j \rangle = \langle \cos(\theta_j - \theta_i) \rangle$ and by assuming that time correlations factorize $\langle \tau_i \tau_j \rangle = \langle \tau_i \rangle \langle \tau_j \rangle$, we obtain a simplified but not trivial expression, that is

$$\langle |\mathbf{x}_n - \mathbf{x}_0|^2 \rangle = n \langle \tau^2 \rangle + 2 \langle \tau \rangle^2 \sum_{i,j>i}^{n} \langle \cos(\theta_j - \theta_i) \rangle \,. \tag{15}$$

The above result is rather general but, as we will discuss later, anomalous or standard behaviour can arise in the limit $n \gg 1$, depending on the asymptotic decay of the Velocity Autocorrelation Function (VACF) to zero. Since the diffusion coefficient is

$$D_{\text{eff}} = \lim_{n\to\infty} \frac{\langle |\mathbf{x}_n - \mathbf{x}_0|^2 \rangle}{2\, n \langle \tau \rangle},$$

one obtains

$$D_{\text{eff}} = \frac{1}{2} \frac{\langle \tau^2 \rangle}{\langle \tau \rangle} + \langle \tau \rangle \sum_{k=1}^{\infty} \langle \cos(\theta_k - \theta_0) \rangle \,. \tag{16}$$

As shown in Appendix A, the hypothesis that angles formed by two consecutive velocities $\phi_k = \theta_{k+1} - \theta_k$ are independent and identically distributed variables leads to the final expression in closed-form

$$D_{\text{eff}} = \frac{1}{2} \frac{\langle \tau^2 \rangle}{\langle \tau \rangle} + \langle \tau \rangle \, \frac{\alpha(1-\alpha) - \beta^2}{(1-\alpha)^2 + \beta^2}, \tag{17}$$

where we set $\alpha = \langle \cos(\phi) \rangle$, $\beta = \langle \sin(\phi) \rangle$ and

$$D_0 = \frac{1}{2} \frac{\langle \tau^2 \rangle}{\langle \tau \rangle} \tag{18}$$

being the independent free-path contribution, also known as random phase approximation (RPA) or quasilinear approximation (QLA) [36,37]. The variation of D_0 with δ is represented by the black triangles in Fig. 5.

It is clear that the particular shape of the profile enters in the values of the constants α, β that are functions of δ. A simple estimate of α, β can be found at the end of the Appendix A leading to the approximated formula

$$D_{\text{eff}} = D_0 + \langle \tau \rangle \frac{\mu(2 - \sqrt{1+\epsilon^2})}{(1+\mu)\sqrt{1+\epsilon^2} - 2\mu} \,, \tag{19}$$

with $\langle \tau \rangle$ taken from Eq. (9) and $\mu = \langle \cos(2\theta) \rangle$ where θ is the angle that the particle velocity forms with channel axis.

Although formula (19) is derived upon strong simplifying assumptions, it is able to catch the basic dependence of the diffusion

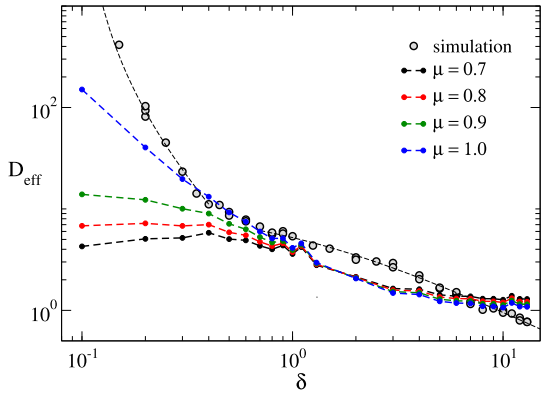

Fig. 6. (Colour online.) Comparison of Eq. (19) (dot-dashed) to simulation data (circles), at different values of the parameter $\mu = \langle \cos(2\theta) \rangle$. Despite the simplifications, Eq. (19) qualitatively reproduces the behaviour of the simulated D_{eff}.

constant on the parameter δ, as it can be seen in Fig. 6. The approximation is expected to reasonably works in the range $\delta > 0.5$ where the corrugation is able to produce enough shuffling in the velocity directions that their correlations can be considered weak.

The correction to D_0 depends parametrically on μ which, either can be left as a free adjustable parameter or it can be estimated from the simulations. Anyway, as Fig. 6 testifies, for $\delta > 0.5$ the dependence on μ is quite weak, and a reasonable agreement is achieved between simulations and theoretical approximation of D_{eff}.

Formula (17) allows also interesting considerations about the diffusion-like mechanism. The second term, accounting for correlations of free-paths before and after a collision, is expected to become relevant as soon as the dynamics develops persistence, for instance when long ballistic flights have a non negligible role. A simple, but not trivial scenario is the following: each trajectory is characterized by a certain persistence, for which it undergoes many forward collisions and few backward ones so that the angular distribution can be considered approximately bimodal

$$p(\phi) = p\delta(\phi) + (1-p)\delta(\phi - \phi_0) \tag{20}$$

with p probability of a forward scattering and $1-p$ the probability to get a backward scattering of an angle $\phi_0 \neq 0$

$$\alpha = \langle \cos(\phi) \rangle = p + (1-p)\cos(\phi_0)$$
$$\beta = \langle \sin(\phi) \rangle = (1-p)\sin(\phi_0).$$

Upon inserting the above expression in Eq. (17), one obtains after simple algebra,

$$D_{\text{eff}} = D_0 + \langle \tau \rangle \, \frac{p - 1/2}{1-p} \,. \tag{21}$$

In the regimes where the dynamics develops strong degree of persistence, $p \simeq 1$, the second term becomes dominant and very large. This elementary argument explains the emergence of the singular behaviour observed in Fig. 5 for small δ.

The behaviour $D_{\text{eff}} \sim 1/\delta$ observed for large values of δ, Eq. (13), can be explained via a simple phenomenological argument discussed in [38–40]. With reference to Fig. 1, the channel can be separated into two regions: the corridor $\mathcal{C}$ and the hump region $\mathcal{H}$. More precisely such regions are defined as

$$\mathcal{C} = \{(x, y) \in \mathbf{R} \mid 0 < y < w_0\} \tag{22}$$

$$\mathcal{H} = \{(x, y) \in \mathbf{R} \mid w_0 < y < w(x)\} \,. \tag{23}$$

Particles spend time both in $\mathcal{C}$ and $\mathcal{H}$ with certain probabilities, but only the time spent in the corridor $\mathcal{C}$ really contributes to

the transport. The msd of the particles that remain in $\mathcal{C}$ is given asymptotically by $\sigma^2(t) \sim 2P_t(\mathcal{C})t$, where $P_t(\mathcal{C})$ is the time dependent survival probability in $\mathcal{C}$.

Since in the long time limit the transverse motion becomes stationary, the occupation probability $P_{\rm eq}(\mathcal{H})$ of $\mathcal{H}$ is

$$P_{\rm eq}(\mathcal{H}) = \frac{\mu(\mathcal{H})}{\mu(\mathcal{H}) + \mu(\mathcal{C})}\,, \tag{24}$$

where $\mu(\mathcal{C}) + \mu(\mathcal{H}) = L(w_0 + \delta/2)$ and $\mu(\mathcal{C}) = Lw_0$ are the geometrical areas within a single period of the channel. Accordingly, the occupation of $\mathcal{C}$ will have probability $P_{\rm eq}(\mathcal{C}) = 1 - P_{\rm eq}(\mathcal{H})$. Thus, the longitudinal motion of a particle can be regarded as a random walk jumping between $\mathcal{C}$ and $\mathcal{H}$ and vice-versa. Within this drastic approximation, the diffusion coefficient is

$$D_{\rm eff} \sim P_{\rm eq}(\mathcal{C}) = \frac{w_0}{w_0 + \delta/2} \tag{25}$$

which explains the $1/\delta$ behaviour as shown in Fig. 5 for large δ, and roughly justifies the fitting function (13).

It is interesting to notice that the approximation (19) for $D_{\rm eff}$ involves two terms; one is coming from the RPA, and the other from the VACF. For $\delta < 3$, the VACF is positive and provides the largest contribution to $D_{\rm eff}$, especially for values δ near to δ_c. While for $\delta > 3$ the contribution of the VACF is mainly negative and reduces the value $D_{\rm eff}$ with respect to D_0. Negative correlations are associated with large number of reflections that a trajectory undergoes, when it remains trapped in the large humps of the wavy profile.

Let us reconsider Eq. (19) which requires some important remarks, as it needs two conditions to be meaningful:

i) finiteness of the second moment of collision times, $\langle\tau^2\rangle$;
ii) convergence of the infinite series $\sum_n \langle \mathbf{v}_0 \cdot \mathbf{v}_n\rangle$.

In principle since our channel has an infinite horizon $\langle\tau^2\rangle$ should logarithmically diverge as shown by [41,42] and discussed in [43]. At a practical level, the actual divergence depends on the chosen initial conditions of the particle ensemble. With the used initial condition the logarithmic divergence which is particularly weak, is not appreciable.

Once one accepts that $\langle\tau^2\rangle$ has "finite" values, there is another delicate issue coming from the sum of velocity auto-correlation $C(n) = \langle \mathbf{v}_0 \cdot \mathbf{v}_n\rangle$. There are two possibilities: i) $C(n)$ decays fast enough to give a finite $D_{\rm eff}$ ii) $C(n)$ decays too slowly, this corresponds to anomalous super diffusion. The most common case (standard diffusion) corresponds to the validity of the central-limit theorem hypothesis. If VACF decays as $C(n) \sim n^{-\beta}$ with $\beta \leq 1$, the diffusion turns to be anomalous, specifically if $\beta < 1$ we have $\sigma^2(t) \sim t^{2-\beta}$ and if $\beta = 1$, $\sigma^2(t) \sim t\ln(t)$ which is a weak form of anomalous diffusion.

It is important to remark that the description of a process just in terms of the asymptotic behaviour of $\sigma^2(t)$ is not always complete, indeed it is meaningful only when the central limit theorem can be applied [44,45]. There are examples of more complex processes that are fully characterized by the knowledge of the whole spectrum of moments $\langle |x(t)|^q\rangle \sim t^{q\nu(q)}$. This corresponds to a failure of the self-similarity [46] for which a single exponent is not enough to describe the diffusive properties of the system. This behaviour is called "strong anomalous diffusion", it is not a mere curiosity and has been observed in several symplectic dynamics [47–49]. In our system, we have numerical evidence of the validity of the most common scenario, i.e. the standard Gaussian diffusion at least in high corrugation conditions. In contrast, several works [41,50–53] agree on the fact that the infinite horizon implies a correlation decay $1/t$ leading to the so-called "marginal anomalous" behaviour $\sigma^2(t) \sim t\ln(t)$. However, it is rather difficult to obtain a sufficiently clean simulation data confirming the presence of the logarithmic multiplier in agreement with the numerical results by Cristadoro et al. [54].

5. Conclusions

We studied numerically the diffusive transport of free particles in a infinite-long channel bounded by a flat and by a periodically corrugated wall; particles hitting the boundaries are mirror reflected. In particular, we investigated the effect of the periodic corrugation on the transport along the channel axis, by varying the parameter δ in the undulating profile (1).

For a large range of δ, we evolved an ensemble of particles initially localized at random along the boundaries of the fundamental cell around the origin. For this set of particles, we first computed the average collision time (mean-free path) making a comparison with the theoretical prediction derived by a simple geometrical argument [27,28].

We also studied the time-behaviour of the mean square displacement $\sigma^2(t)$ of the particles from their initial conditions which, despite the infinite horizon, exhibits an asymptotic behaviour which cannot be distinguished from a genuine diffusion. An effective diffusion coefficient $D_{\rm eff}$ is obtained showing an interesting dependence on the parameter δ. In fact, $D_{\rm eff}$ has an overall monotonic decrease when δ increases, but there is a threshold δ_c below which the ballistic motion of the particles prevails leading to a $\sigma^2(t) \sim t^2$ behaviour. Simulation results indicate that for moderate and large δ, $D_{\rm eff}$ decreases as $1/\delta$. The large corrugation regime enhances the trapping action of the humps, because the particles may frequently collide with the hump walls, this decreases the statistical occupation of the corridor thus reducing somehow the pathological effects of the infinite horizon.

Let us conclude with a comment the consequences of the infinite horizon, because the presence of the corridor allows free flights of arbitrary length. According to the works [41,49–51] this condition is mathematically sufficient for a system to show "marginal anomalous diffusion" characterized by a msd $\sigma^2(t) \sim t\ln(t)$ corresponding to a ill-defined diffusion coefficient which diverges as $\ln(t)$. Although our simulations evolved 2×10^4 particles for a time window $T_w = 10^6$, we were not able to really appreciate logarithmic deviations from the standard diffusion.

Presumably such difficulty, discussed also in Ref. [54,55], can be primarily ascribed not only to the weakness of $\ln(t)$ correction, whose detection is easily shaded by finite time/size effects and by the selection of the initial conditions, but also to the "uncertainty" of the evolution algorithm due to the small but finite accuracy in the numerical solution of Eq. (5). Likely, these factors concur to the suppression of arbitrary long flights that soon or later turn to be re-absorbed. This situation virtually corresponds to the presence of a "external noise" that eventually regularizes the singularities of the second moment of the collision-time distribution as well as of the mean square displacement.

Acknowledgements

The work of G.G.; A.V.; and V.B. is supported through the Royal Society International Exchange Grant (Grant-Num.: IE150198), EPSRC (Grant-Ref.: EP/K019694/1), and EU Horizon 2020 FET "NEMF21" (Grant-Num.: 664828). F.C. was supported by the Grant "Fondi Ateneo 2015" from University "Sapienza" Rome, Italy.

The authors warmly thank M. Bernaschi, A. Cavagna and A. Taloni for useful suggestions and discussions. Moreover the authors express their gratitude to R. Artuso and C.P. Dettmann for a critical reading of the manuscript.

Appendix A

In this appendix we compute the sum over the angles in formula (15)

$$F_n = \sum_{i,j>i}^{n} \langle \cos(\theta_j - \theta_i) \rangle$$

expanding the double summation

$$F_n = \sum_{i=1}^{n-1} \left[\sum_{j=i+1}^{n} \langle \cos(\theta_j - \theta_i) \rangle \right]$$

and changing the index $k = j - i$, $(1 \le k \le n - i)$,

$$F_n = \sum_{i=1}^{n-1} \left[\sum_{k=1}^{n-i} \langle \cos(\theta_{k+i} - \theta_i) \rangle \right] \tag{A.1}$$

the argument of the cosine can be written as a sum of consecutive angular increments $\theta_{l+1} - \theta_l = \phi_l$

$$\theta_{k+i} - \theta_i = \sum_{l=i}^{i+k-1} (\theta_{l+1} - \theta_l) = \sum_{l=1}^{k} \phi_l$$

therefore we have

$$\langle \cos(\theta_{k+i} - \theta_i) \rangle = \left\langle \cos \left[\sum_{l=1}^{k} \phi_l \right] \right\rangle .$$

The assumption that the angular increments, ϕ_l, are independent and identically distributed implies that the above expression can be re-written as

$$\langle \cos(\theta_{i+k} - \theta_i) \rangle = \frac{1}{2} \left[\langle e^{i\phi} \rangle^k + \langle e^{-i\phi} \rangle^k \right].$$

If we set $z = \langle e^{i\phi} \rangle$ and $\overline{z} = \langle e^{-i\phi} \rangle$, the sum running on k in Eq. (A.1) reduces to

$$\sum_{k=1}^{n-i} \langle \cos(\theta_{k+i} - \theta_i) \rangle = \sum_{k=1}^{n-i} \frac{1}{2} \left(z^k + \overline{z}^k \right),$$

then, using the geometric series formulas, we obtain

$$\sum_{k=1}^{n-i} \langle \cos(\theta_{k+i} - \theta_i) \rangle = \frac{1}{2} \left[z \frac{1 - z^{n-i}}{1 - z} + \overline{z} \frac{1 - \overline{z}^{n-i}}{1 - \overline{z}} \right].$$

Finally developing the sum on i in Eq. (A.1),

$$F_n = \frac{z/2}{1 - z} \left[n - \frac{1 - z^n}{1 - z} \right] + \frac{\overline{z}/2}{1 - \overline{z}} \left[n - \frac{1 - \overline{z}^n}{1 - \overline{z}} \right] \tag{A.2}$$

In the limit of large n, the leading contribution is

$$F_n \sim \frac{n}{2} \left[\frac{z}{1 - z} + \frac{\overline{z}}{1 - \overline{z}} \right] = n \Re \left[\frac{z}{1 - z} \right]$$

where the coefficient $F = \Re \{ z/(1 - z) \}$, after expressing $z = \langle \cos(\phi) \rangle + i \langle \sin(\phi) \rangle$, becomes

$$F = \frac{\alpha(1 - \alpha) - \beta^2}{(1 - \alpha)^2 + \beta^2}$$

and provides the result (17), with $\alpha = \langle \cos(\phi) \rangle$ and $\beta = \langle \sin(\phi) \rangle$.

We now attempt an estimate of α and β. This can be achieved by considering the transfer matrix (6) which relates the pre-collision velocity $\mathbf{v} = (\cos\theta, \sin\theta)$ to the post-collision one $\mathbf{v}' = M\mathbf{v}$. By definition $\alpha = \langle \mathbf{v} \cdot \mathbf{v}' \rangle = \langle \mathbf{v} \cdot M\mathbf{v} \rangle$ and $\beta = \langle \mathbf{v} \times \mathbf{v}' \rangle$.

Now, because the elements of each row of M are bounded between $[-1, 1]$ and satisfy the condition $M_{r,x}^2 + M_{r,y}^2 = 1$, M can be easily re-parameterized as

$$M = \begin{bmatrix} \cos\eta & \sin\eta \\ \sin\eta & -\cos\eta \end{bmatrix}, \tag{A.3}$$

where we have set,

$$\cos\eta = \frac{2}{1 + m^2} - 1, \quad \text{and} \quad \sin\eta = \frac{2m}{1 + m^2} .$$

A simple algebraic manipulation gives $\alpha = \langle \cos(\eta - 2\theta) \rangle$ and likewise $\beta = \langle \sin(\eta - 2\theta) \rangle$. As a consequence, the "angle" η is related to the angle ϕ (between two consecutive velocities) via the equation $\phi = \eta - 2\theta$.

Expanding the trigonometric expressions of α and β, and assuming the averages over η and θ to be factorized, we obtain

$$\alpha = \langle \cos\eta \rangle \langle \cos(2\theta) \rangle + \langle \sin\eta \rangle \langle \sin(2\theta) \rangle$$

$$\beta = \langle \sin\eta \rangle \langle \cos(2\theta) \rangle - \langle \cos\eta \rangle \langle \sin(2\theta) \rangle .$$

In addition, due to the channel symmetry, we can set $\langle \sin\eta \rangle = \langle \sin(2\theta) \rangle = 0$, thus

$$\alpha = \langle \cos\eta \rangle \langle \cos(2\theta) \rangle \quad \text{and} \quad \beta = 0 .$$

According to the definitions (1), (6) and by assuming a uniform distribution of x on the unitary cell,

$$\langle \cos\eta \rangle = \frac{4}{L} \int_0^{L/2} \frac{dx}{1 + \epsilon^2 \sin^2(kx)} - 1$$

with $\epsilon = \pi\delta/L$, and after a simple integration, we obtain

$$\langle \cos\eta \rangle = \frac{2}{\sqrt{1 + \epsilon^2}} - 1 = A , \tag{A.4}$$

leading to the expression

$$F = \frac{A \langle \cos(2\theta) \rangle}{1 - A \langle \cos(2\theta) \rangle} .$$

Finally by denoting $\mu = \langle \cos(2\theta) \rangle = \langle \cos^2\theta \rangle - \langle \sin^2\theta \rangle$ and using (A.4), we arrive at the result

$$F = \frac{\mu(2 - \sqrt{1 + \epsilon^2})}{(1 + \mu)\sqrt{1 + \epsilon^2} - 2\mu} , \tag{A.5}$$

representing a correction to the RPA diffusion coefficient, D_0, only due to the correlation between the velocity before and after a collision with the corrugated wall. The correction depends parametrically on μ, but as Fig. 6 shows, such a dependence is also weak. In the absence of reasonable guesses on the values of μ, it can be left as an adjustable parameter.

References

[1] P. Aschieri, V. Doya, A. Picozzi, Complex behaviour of a ray in a Gaussian index profile periodically segmented waveguide, J. Opt. A, Pure Appl. Opt. 8 (5) (2006) 386.

[2] A.G. York, H.M. Milchberg, J.P. Palastro, T.M. Antonsen, Direct acceleration of electrons in a corrugated plasma waveguide, Phys. Rev. Lett. 100 (May 2008) 195001.

[3] Ruey Bing Hwang, Negative group velocity and anomalous transmission in a one-dimensionally periodic waveguide, IEEE Trans. Antennas Propag. 54 (Feb 2006) 755–760.

[4] I.L. Garanovich, S. Longhi, A.A. Sukhorukov, Y.S. Kivshar, Light propagation and localization in modulated photonic lattices and waveguides, Phys. Rep. 518 (2012) 1–79.

[5] C. Michel, M. Allgaier, V. Doya, Regular modes in a mixed-dynamics-based optical fiber, Phys. Rev. E 93 (Feb 2016) 022201.
[6] E. Rousseau, D. Felbacq, Ray chaos in a photonic crystal, Europhys. Lett. 117 (2017) 14002.
[7] G. Tanner, Dynamical energy analysis: determining wave energy distributions in vibro-acoustical structures in the high-frequency regime, J. Sound Vib. 320 (2009) 1023–1038.
[8] G. Gradoni, S.C. Creagh, G. Tanner, C. Smartt, D.W.P. Thomas, A phase-space approach for propagating field–field correlation functions, New J. Phys. 17 (9) (2015) 093027.
[9] S.C. Creagh, G. Gradoni, T. Hartmann, G. Tanner, Propagating wave correlations in complex systems, J. Phys. A, Math. Theor. 50 (2017) 045101 (1–18).
[10] C.W.J. Beenakker, H. van Houten, Billiard model of a ballistic multiprobe conductor, Phys. Rev. Lett. 63 (Oct 1989) 1857–1860.
[11] D. Alonso, R. Artuso, G. Casati, I. Guarneri, Heat conductivity and dynamical instability, Phys. Rev. Lett. 82 (1999) 1859.
[12] I.F. Herrera-González, H.I. Pérez-Aguilar, A. Mendoza-Suárez, E.S. Tututi, Heat conduction in systems with Kolmogorov–Arnold–Moser phase space structure, Phys. Rev. E 86 (2012) 031138.
[13] P. Gaspard, What is the role of chaotic scattering in irreversible processes?, Chaos 3 (1993) 427–442.
[14] P.M. Bleher, Statistical properties of a particle moving in a periodic scattering billiard, in: W. Kasprzak, A. Weron (Eds.), Stochastic Methods in Experimental Science, World Sci. Publ., River Edge, NJ, 1990, pp. 43–58.
[15] D.P. Sanders, Fine structure of distributions and central limit theorem in diffusive billiards, Phys. Rev. E 71 (2005) 016220.
[16] M. Horvat, T. Prosen, Uni-directional transport properties of a serpent billiard, J. Phys. A, Math. Gen. 37 (2004) 3133.
[17] E.D. Leonel, Corrugated waveguide under scaling investigation, Phys. Rev. Lett. 98 (2007) 114102.
[18] E.D. Leonel, D.R. da Costa, C.P. Dettmann, Scaling invariance for the escape of particles from a periodically corrugated waveguide, Phys. Lett. A 376 (2012) 421–425.
[19] D.R. da Costa, M.R. Silva, E.D. Leonel, Escape beam statistics and dynamical properties for a periodically corrugated waveguide, Commun. Nonlinear Sci. Numer. Simul. 19 (2014) 842–850.
[20] D.P. Sanders, H. Larralde, Occurrence of normal and anomalous diffusion in polygonal billiard channels, Phys. Rev. E 73 (2006) 026205.
[21] O.G. Jepps, C. Bianca, L. Rondoni, Onset of diffusive behavior in confined transport systems, Chaos 18 (2008) 013127.
[22] D. Alonso, A. Ruiz, I. de Vega, Polygonal billiards and transport: diffusion and heat conduction, Phys. Rev. E 66 (2002) 066131.
[23] F. Cecconi, D. del Castillo-Negrete, M. Falcioni, A. Vulpiani, The origin of diffusion: the case of non-chaotic systems, Phys. D: Nonlinear Phenom. 180 (2003) 129–139.
[24] F. Cecconi, M. Cencini, A. Vulpiani, Transport properties of chaotic and non-chaotic many particle systems, J. Stat. Mech. Theory Exp. 2007 (2007) P12001.
[25] R.S. Mackay, J.D. Meiss, I.C. Percival, Transport in Hamiltonian systems, Physica D 13 (1984) 55–81.
[26] A.F. Rabelo, E.D. Leonel, Finding invariant tori in the problem of a periodically corrugated waveguide, Braz. J. Phys. 38 (2008) 54–57.
[27] N. Chernov, Entropy, Lyapunov exponents, and mean free path for billiards, J. Stat. Phys. 88 (1997) 1–29.
[28] V.B. Kokshenev, E. Vicentini, Physical insight into superdiffusive dynamics of Sinai billiard through collision statistics, Phys. A, Stat. Mech. Appl. 360 (2006) 197–214.
[29] M. Abramowitz, I.A. Stegun, Handbook of Mathematical Functions with Formulas, Graphs, and Mathematical Tables, 10th ed., Dover Publications Inc., New York, 1972.
[30] B.V. Chirikov, A universal instability of many-dimensional oscillator systems, Phys. Rep. 52 (1979) 263.
[31] S. Grossmann, H. Fujisaka, Diffusion in discrete nonlinear dynamical systems, Phys. Rev. A 26 (1982) 1779.
[32] T. Geisel, J. Nierwetberg, Onset of diffusion and universal scaling in chaotic systems, Phys. Rev. Lett. 48 (1982) 7–10.
[33] R. Klages, N. Korabel, Understanding deterministic diffusion by correlated random walks, J. Phys. A, Math. Gen. 35 (2002) 4823.
[34] T. Gilbert, D.P. Sanders, Persistence effects in deterministic diffusion, Phys. Rev. E 80 (Oct 2009) 041121.
[35] P.M. Kareiva, N. Shigesada, Analyzing insect movement as a correlated random walk, Oecologia 56 (1983) 234–238.
[36] A.N. Yannacopoulos, G. Rowlands, Calculation of diffusion coefficients for chaotic maps, Phys. D: Nonlinear Phenom. 65 (1993) 71–85.
[37] J.R. Cary, J.D. Meiss, Rigorously diffusive deterministic map, Phys. Rev. A 24 (1981) 2664.
[38] L. Dagdug, A.M. Berezhkovskii, Y.A. Makhnovskii, V.Yu. Zitserman, Transient diffusion in a tube with dead ends, J. Chem. Phys. 127 (2007) 224712.
[39] A.M. Berezhkovskii, L. Dagdug, Analytical treatment of biased diffusion in tubes with periodic dead ends, J. Chem. Phys. 134 (2011) 124109.
[40] G. Forte, F. Cecconi, A. Vulpiani, Transport and fluctuation-dissipation relations in asymptotic and preasymptotic diffusion across channels with variable section, Phys. Rev. E 90 (2014) 062110.
[41] P.M. Bleher, Statistical properties of two-dimensional periodic Lorentz gas with infinite horizon, J. Stat. Phys. 66 (1992) 315–373.
[42] D. Szász, T. Varjú, Limit laws and recurrence for the planar Lorentz process with infinite horizon, J. Stat. Phys. 129 (2007) 59–80.
[43] C.P. Dettmann, Diffusion in the Lorentz gas, Commun. Theor. Phys. 62 (2014) 521–540.
[44] J. Klafter, I.M. Sokolov, First Steps in Random Walks: From Tools to Applications, Oxford University Press, 2011.
[45] R. Klages, G. Radons, I.M. Sokolov (Eds.), Anomalous Transport: Foundations and Applications, John Wiley & Sons, 2008.
[46] P. Castiglione, A. Mazzino, P. Muratore-Ginanneschi, A. Vulpiani, On strong anomalous diffusion, Physica D 134 (1999) 75–93.
[47] R. Artuso, G. Cristadoro, Anomalous transport: a deterministic approach, Phys. Rev. Lett. 90 (2003) 244101.
[48] R. Artuso, L. Cavallasca, G. Cristadoro, Dynamical and transport properties in a family of intermittent area-preserving maps, Phys. Rev. E 77 (2008) 046206.
[49] D.N. Armstead, B.R. Hunt, E. Ott, Anomalous diffusion in infinite horizon billiards, Phys. Rev. E 67 (2003) 021110.
[50] P. Dahlqvist, R. Artuso, On the decay of correlations in Sinai billiards with infinite horizon, Phys. Lett. A 219 (1996) 212–216.
[51] B. Friedman, R.F. Martin Jr., Decay of the velocity autocorrelation function for the periodic Lorentz gas, Phys. Lett. A 105 (1984) 23–26.
[52] L.A. Bunimovich, Decay of correlations in dynamical systems with chaotic behavior, JEPT 89 (1985) 1452–1471.
[53] A. Zacherl, T. Geisel, J. Nierwetberg, G. Radons, Power spectra for anomalous diffusion in the extended Sinai billiard, Phys. Lett. A 114 (1986) 317–321.
[54] G. Cristadoro, T. Gilbert, M. Lenci, D.P. Sanders, Measuring logarithmic corrections to normal diffusion in infinite-horizon billiards, Phys. Rev. E 90 (2014) 022106.
[55] C.P. Dettmann, New horizons in multidimensional diffusion: the Lorentz gas and the Riemann hypothesis, J. Stat. Phys. 146 (2012) 181–204.